A Linearly Extendible Multi-Artifact Removal Approach for Improved Upper Extremity EEG-based Motor Imagery Decoding

Mojisola Grace Asogbon[1,2], Oluwarotimi Williams Samuel [1,2,4]*, Xiangxin Li [1,2,4], Ejay Nsugbe[5], Erik Scheme[6], and Guanglin Li [1,2,3,4]*

[1]CAS Key Laboratory of Human-Machine Intelligence-Synergy Systems, Shenzhen Institutes of Advanced Technology (SIAT), Chinese Academy of Sciences (CAS), Shenzhen 518055, China.

[2]Shenzhen College of Advanced Technology, University of Chinese Academy of Sciences, Shenzhen 518055, China.

[3]Guangdong-Hong Kong-Macau Joint Laboratory of Human-Machine Intelligence-Synergy Systems, Shenzhen 518055, China

[4]SIAT Branch, Shenzhen Institute of Artificial Intelligence and Robotics for Society

[5]University of Bristol, Queen's Building, University Walk, Bristol BS8 1TR, UK

[6]Institute of Biomedical Engineering, University of New Brunswick, Fredericton, NB, Canada

Abstract-

Background and Objective: Non-invasive multichannel Electroencephalography (EEG) recordings provide an alternative source of neural information from which motor imagery (MI) patterns associated with limb movement intent can be decoded for use as control inputs for rehabilitation robots. The presence of multiple inherent dynamic artifacts in EEG signals, however, poses processing challenges for brain-computer interface (BCI) systems. A large proportion of the existing EEG signal preprocessing methods focus on isolating single artifact per time from an ensemble of EEG trials and require calibration and/or reference electrodes, resulting in increased complexity of their application to MI-EEG controlled rehabilitation devices in practical settings. Also, a few existing multi-artifacts removal methods though explored in other domains, they have rarely been investigated in the space of MI-EEG signals for multiple artifacts cancellation in a simultaneous manner.

Approach: Building on the premise of previous works, this study propose a semi-automatic EEG preprocessing method that combines Generalized Eigenvalue Decomposition driven by low-rank approximation and a Multi-channel Wiener Filter (GEVD-MWF) that employs a learning technique for simultaneous elimination of multiple artifacts from MI-EEG signals. The proposed method is applied to remove multiple artifacts from 64-channel EEG signals recorded from transhumeral amputees while they performed distinct classes of upper limb MI tasks before decoding their movement intent using a selection of features and machine learning algorithms.

Main Results: Experimental results show that the proposed GEVD-MWF method yields significant improvements in MI decoding accuracies, in the range of 13.23%-41.21% compared to four existing popular artifact removal algorithms. Further investigation revealed that the GEVD-MWF approach enabled accuracies in the range of 90.44% - 99.67% using "single trial" EEG recordings, which could eliminate the need to record and process large ensembles of EEG trials as commonly required in some existing approaches. Additionally, using a variant of the sequential forward floating selection algorithm, a subset of 9 channels was used to obtain a decoding accuracy of 93.73%±1.58%.

Significance: Given its improved performance, reduced data requirements, and feasibility with few channels, the proposed GEVD-MWF could potentially spur the development of effective real-time control strategies for multi-degree of freedom EEG-based miniaturized rehabilitation robotic interfaces.

Keywords: Electroencephalography, Signal processing, Artifact removal, Motor imagery decoding, Pattern recognition, Brain-Computer interface

I. INTRODUCTION

Inspired by the need to develop clinically viable rehabilitation devices for upper limb motor function restoration, particularly in amputees and stroke survivors, several advancements have been made in recent decades. Rehabilitation and assistive devices driven by surface myoelectric pattern recognition (sMPR) have been explored as one possible solution [1-2]. Nonetheless, intuitively dexterous multiple degrees of freedom (MDoFs) myoelectric prostheses built for above-elbow amputees (shoulder disarticulation and transhumeral amputees) have not yet gained wide acceptance among users, partially because of the lack of available muscle sites required to generate the requisite signals for physiologically appropriate control [3]. In addressing this limitation, an alternative signal source is required. The non-invasive electroencephalogram (EEG), characterized by excellent temporal resolution, and the improving ease of acquisition and cost of measurement devices, may soon make it a viable solution [4-5].

Given the above merits, brain-computer-interfaces (BCI) driven by motor imagery (MI) patterns inherent in EEG signals are currently being explored in academia and industry to develop efficient prosthetic control mechanisms for high-level amputees [6]. However, confounding factors including *non-physiological* (artifacts from electrode displacement, electromagnetic interference, and electrical appliances) and *physiological* (artifacts from cardiac, muscle, eye movement, respiratory activities) pose serious processing challenges to EEG signals, thereby degrading the decoding of MI tasks [7-8]. With proper experimental design and adoption of simple filtering techniques, *non-physiological* artifacts can be significantly reduced or even avoided, but *physiological* artifacts caused by eye blinks or movements, cardiac activity, head movements, and muscle activity are more difficult to eliminate, and therefore require the use of dedicated artifact removal algorithms [9-10].

To resolve the impact of *physiological-based* artifacts that are contained in EEG recordings, automated and semi-automated methods inspired by regression, blind source separation (BSS), and filtering techniques have been proposed [7]. For instance, time-domain driven regression techniques have been applied for ocular artifact cancelation in multi-channel EEG recordings [11-14]. Though these techniques have low computational cost, they require the use of at least one reference channel, which in turn undermines their practicality for ocular artifact removal. Principal component analysis (PCA) based approaches were built for ocular artifacts elimination with superior performance than regression-based methods in terms of computational efficiency [**15-17**]. Similarly, techniques driven by independent component analysis (ICA), canonical correlation analysis (CCA), and dipole source analysis (DSA) have been implemented for handling eye blinks, movement-related artifacts, and muscle artifacts in EEG recordings [7,11, 18-21]. However, these BSS methods are based on data-driven transformation concepts and artifact components need to be selected automatically or semi-automatically for removal after source separation. Moreover, they have rarely been explored in the space of MI-EEG signals for multiple artifacts cancellation in a simultaneous manner.

As an alternative approach to resolve the limitations of the BSS and regression-based methods, artifact separation from EEG recordings via filtering and integrated approaches have been explored in recent years [14, 22-23]. Proposed approaches include methods based on automatic artifact correction driven by regression and ICA [24], second and higher-order statistics [25], fully automated statistical thresholding artifact rejection, and multiple artifact rejection

algorithms (MARA) [26]. Though these methods were reported to have achieved improved artifact removal compared to the aforementioned single method approaches, they include drawbacks that have hindered their widespread adoption in practical applications. Generally, these methods are designed for single artifact removal or to eliminate artifacts from known sources and/or require careful calibration that increases the complexity of their application. Additionally, other existing related methods have been successful in eliminating artifacts from EEG recordings by averaging over an ensemble of many trials [7,27]. While effective, this precludes their use in rapid real-time processing of brain signals, particularly in portable systems that include limited memory and processor capabilities. Hence, there remains a need for a computationally efficient multiple artifact removal approach that would address the limitations of current methods. In particular, we hypothesized that the limitation of the existing methods and their non-exploration in the space of MI-EEG recordings for multiple artifacts removal from a single EEG trial could be a major inhibitor to the clinical application of BCI systems; particularly in the field of MDoFs prostheses and in other forms of miniaturized rehabilitation robots.

Therefore, in this study, we propose an MI-EEG preprocessing method using Generalized Eigenvalue Decomposition driven by low-rank approximation and Multi-channel Wiener filter (GEVD-MWF) for simultaneous isolation of multiple artifacts inherent in EEG signals to realize accurate and robust MI task decoding. The GEVD-MWF method employs a semi-supervised artifact learning and filtering technique to accurately estimate EEG signal patterns by isolating and removing inherent artifacts from the original contaminated recordings. In addition to being able to learn and isolate multiple artifact patterns based on prior-marking, the GEVD-MWF method does not require calibration or the use of extra reference channels, which are necessary for some existing methods [7, 12-14, 22]. These attributes make it feasible for our method to handle non-stationary and low SNR (signal to noise ratio) characteristics of the signal, particularly when applied to single-trial EEG recordings from smaller numbers of channels for MI task decoding [28-29]. Furthermore, this study represents one of few works that have investigated the possibility of eliminating multiple artifacts from single-trial MI-EEG recordings for motor imagery pattern decoding from transhumeral amputees. The main contributions of this work are therefore presented as follows:

1. This study describes a robust and effective method (GEVD-MWF) that incorporates a learning technique for simultaneous elimination of multiple artifacts from 64-channel MI-EEG recordings from transhumeral amputees while they performed five distinct classes of upper limb MI tasks.
2. The feasibility of adopting the proposed GEVD-MWF for real-time processing in practical application is demonstrated using a variant of the sequential forward floating selection (vSFFS) algorithm based on the conventional SFFS implementation [30] to select optimal subsets channels out of the 64-channel MI-EEG recordings for robust and accurate MI task decoding. The locations of these electrode channels on the scalp of individual subjects are explored to assess the practicality of precise placement and setup time in practical applications.
3. Lastly, the GEVD-MWF method is demonstrated to yield consistently high MI decoding accuracies using only a single EEG trial across subjects and classifiers, thus providing a potential solution to a key limitation of the existing EEG signal processing methods.

II. MATERIALS AND METHODS

A. Participant Information

The participant recruitment process was preceded by a preliminary evaluation of a set of individuals of which four male transhumeral amputees with residual limb length of 25.50±4.50 cm met the study criteria, and were recruited. The objective of the study and the experimental procedure was carefully described to the participants after which they agreed to take part in the study. The demographic information of the participants is presented in Table 1. The experimental protocol was approved by the Institutional Review Board of Shenzhen Institutes of Advanced Technology, Chinese Academy of Sciences with a reference identification number of SIAT-IRB-150515-H0077. The authors have confirmed that any identifiable participants in this study have given their consent for publication.

Table 1: Participants information recruited for this study

Participants ID	*Trans-H1*	*Trans-H2*	*Trans-H3*	*Trans-H4*
Age in Years	49	46	35	36
Amputation Side	Left	Left	Right	Right
Length of Residuum	20	25	27	30
Years of Amputation	3	9	5	7

Note: The length of residuum was measured from the shoulder blade downwards. Trans-H1 to Trans-H4 denote the four transhumeral amputees

.

B. Signal Collection and Processing

A 64-channel Al-AgCl EEG recording system (EasyCap Brain Products GmbH, Germany) using a Neuroscan System (Version 4.3) was employed to acquire signal from the participants. After a preliminary assessment of the participants, the EEG electrodes were distributed over the scalp of each subject based on the international 10-20 electrode placement configuration as shown in Figure 1.

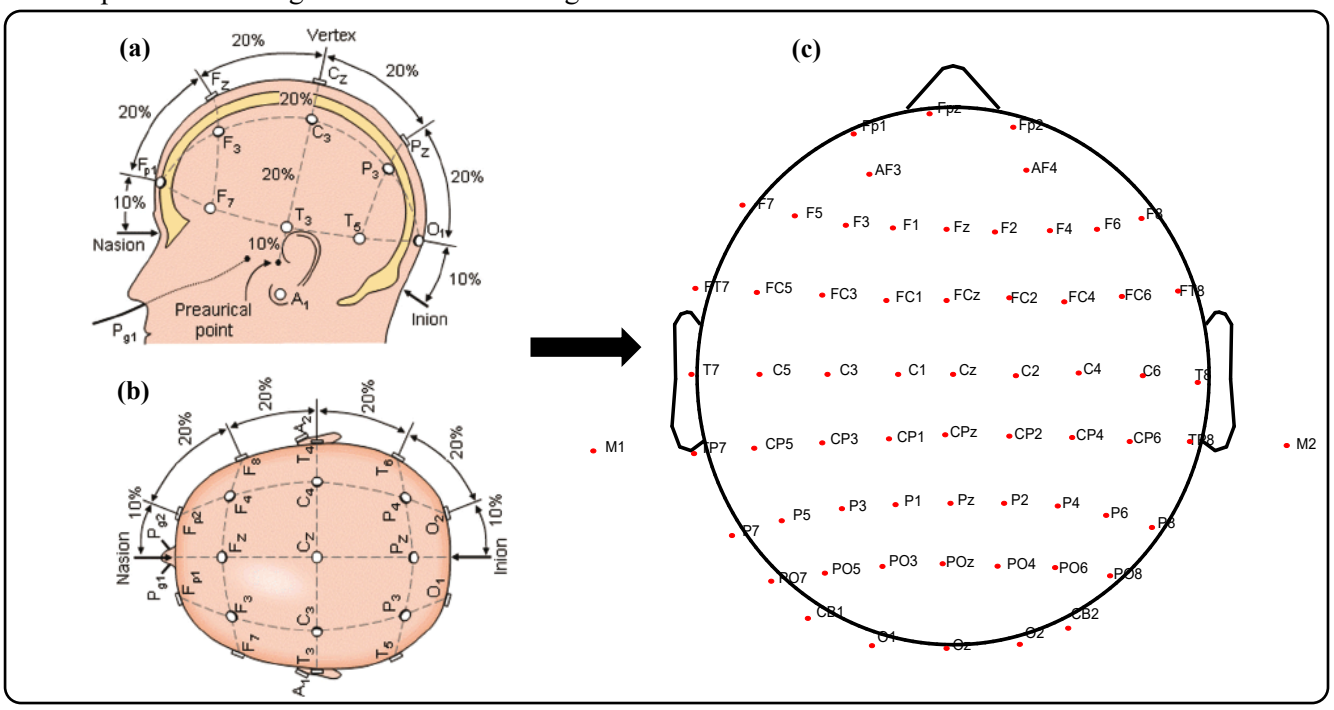

Figure 1: Representation of 64 electrode configuration using the international 10-20 system seen from (a) sagittal and (b) axial plane (c) the scalp perspectives. NOTE: A= ear lobe, C = central, Pg = nasopharyngeal, P = parietal, F = frontal, Fp = frontal polar and O = occipital.

Preceding the placement of the 64-electrode cap, each subject's hair was washed with soap and dried with a towel while the electrode cap position was adjusted accordingly. The impedance between each electrode and a subject's scalp was ensured to be below 10 kΩ to achieve sufficiently high signal quality. Before the experiment, the subjects were given a short training period to accustom themselves to the experimental procedure. Five motor imagery tasks, comprised of hand close (HC), hand open (HO), wrist pronation (WP), wrist supination (WS), and no movement (NM), were used for this experiment. During the experimental session, a computer screen was placed in front of the subjects to display an image of each class of the motor imagery task in random order. When an image appeared on the screen, the subjects were asked to imagine eliciting the corresponding MI task for 5s until the image disappeared. A 5s rest period was given between each set of images to elicit a rest state in the imagination process and avoid mental fatigue. Five full sessions were completed by each subject, each consisting of 40 active MI tasks (10 randomly ordered repetitions of each MI task) plus 40 repetitions of NM. It should be noted that the integrated Neuroscan Software mentioned above was configured to automatically mark a vertical line on the EEG recordings as the onset/offset points of each specified motor imagery task, triggered when a corresponding limb movement image appears/disappears on/from the computer screen in front of a subject.

The MI-EEG signals were recorded at a sampling rate of 1000 Hz, after which the EEGLAB toolbox (version 13.4.4b) was used to extract the epochs corresponding to the various classes of MI tasks. For each task, the 5s recordings plus the 120ms of recordings preceding the task onset were extracted, totaling 5120 data points. The proposed GEVD-MWF method was then used to clean up the epoched signals from multiple inherent artifacts to allow informative and discriminative features to be extracted. This was implemented in two stages. The first stage involved the use of a graphical user interface to visualize the signals and identify a set of multi-artifact exemplars for segmentation/marking. In the second stage, the time indices of the markings were exported to MATLAB where they were used to remove the marked artifact segments with the aid of an integrated Multi-Weiner Filter.

The mathematical model of the recorded signals is presented in equation (1) and the conceptual framework of the proposed MI-EEG based pattern recognition system is shown in Figure 2.

$$x_{EEG\_r(t)} = \sum_{r=1}^{n} x_r(t) + a_r(t) \tag{1}$$

where $x_{EEG\_r(t)}$ represents the recorded EEG signals per trial, x_r is the signal from the r^{th} channel, $a(r)$ is the artifact in the recorded signal and n is the total number of electrode channels used (n = 64).

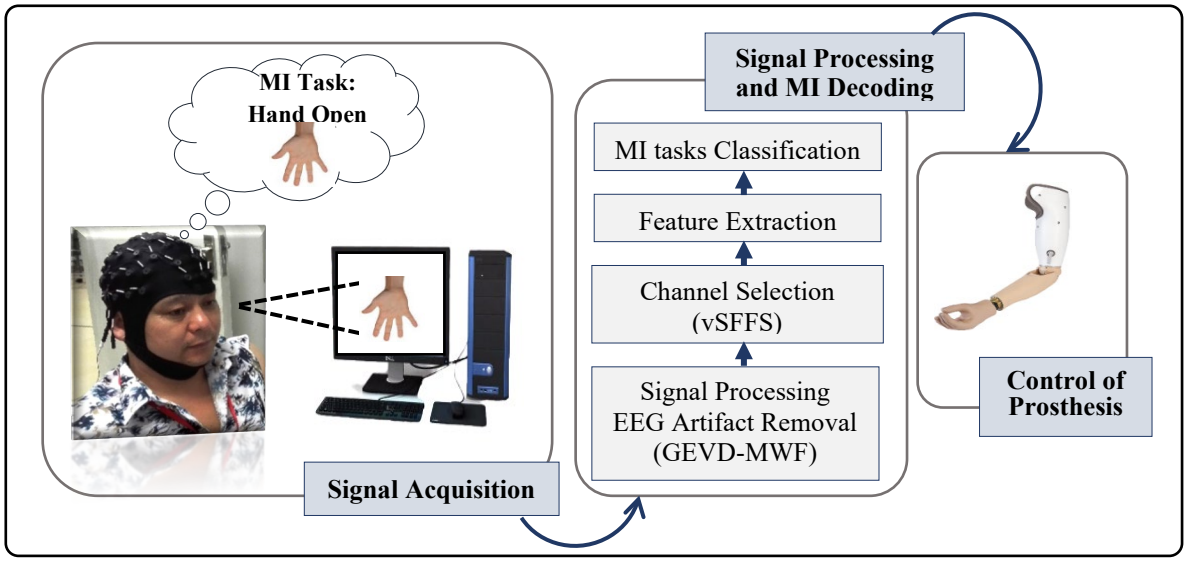

Figure 2: A conceptual framework of the proposed GEVD-MWF and MI-EEG pattern recognition model

C. *Signal Modelling for MWF*

Suppose the recorded MI-EEG signals, $z[t] \in P^M$ at a sampling time, *t*, is given as

$$z[t] = x[t] + y[t] \tag{2}$$

where $x[t] \in P^M$ represent a vector P of dimension M that contains the real neural signals and $y[t]$ denotes different types of artifacts (such as ocular, cardiac, and muscle activities) inherent in the original neural signals (z[t]). The signals $z[t], x[t]$ and $y[t]$ observed at a particular sample time $t \in N,$ are treated as stochastic *N*-dimensional vectors and for conciseness, sample index *t* is preserved in the subsequent equations. Because mean subtraction is a common first preprocessing step, signals *z*, *x*, and *y* are assumed to be of zero-mean, as is often satisfied for EEG signals. Subsequently, the covariance matrices of the signals represented as: P_{zz}, P_{xx} and P_{yy}, are defined as $E\{zz^T\}$, $E\{xx^T\}$, and $E\{yy^T\}$, respectively, where $E\{.\}$ is the expected value operator. With the assumption that x and y are not correlated, then a relationship is formulated as:

$$P_{zz} = P_{xx} + P_{yy} \tag{3}$$

By linearly combining the channels of *z*, the MWF generates an estimate ($\hat{y}$) of the multi-channel artifact signals *y*, that is $\hat{y} = W^T \mathrm{z}$ where W is the linear estimator and superscript $^{\mathrm{T}}$ is the conjugate transpose operator. The linear combination above was optimized using the *mean square error* criterion in equation (4).

$$W^T = \arg\min_{w} E\{\|y - W^T \mathrm{z}\|^2\} \tag{4}$$

Assuming $P_{zz} = E\{zz^T\}$ has full rank, the unique solution in equation (4) becomes:

$$W = P_{zz}^{-1} P_{zy} \tag{5}$$

where $P_{zy} = E\{zy^T\}$. Recall from equation (2) that $z = x + y$ and assuming y and x are not correlated, then $P_{zy} = P_{yy}$, as given by:

$$P_{zy} = P_{(x+y)y} = P_{xy} + P_{yy} = P_{yy} \tag{6}$$

Consequently, the filter solution from equation (5) can be represented as:

$$W = P_{zz}^{-1} P_{yy} \tag{7}$$

Practically, the signal correlation matrix P_{zz} is often not available, but it can be estimated using a sample averaging technique. Hence, the $M \times T$ observation matrix Z can be defined, where the t^{th} column corresponds to an observation of *z[t]* at a particular time. Using an artifact detection approach (GUI based approach), the T observations of Z were separated into mutually exclusive sets, Z_a and Z_b, where the first set contains T_a artifact contaminated samples while the second set contains T_b artifact-free samples [31]. This process allows P_{zz} to be estimated as:

$$\hat{P}_{zz} = \frac{1}{T_a} Z_a Z_a^T \tag{8}$$

where the circumflex (‘ˆ’) accent symbol denotes the estimation. Comparably, from $M \times T_b$ observation matrix Z_b, containing artifact-free samples, P_{xx} is estimated as:

$$\hat{P}_{xx} = \frac{1}{T_b} Z_b Z_b^T \tag{9}$$

Based on equation (3), an estimate of P_{yy} can be determined as shown in equation (10). Meanwhile, the filter solution W from equation (7) can be calculated using the covariance matrix estimates as shown in equation (11).

$$\hat{P}_{yy} = \hat{P}_{zz} - \hat{P}_{xx} \tag{10}$$

$$\widehat{W} = \hat{P}_{zz}^{-1} \hat{P}_{yy} \tag{11}$$

By subtracting the estimated artifacts using the additive model of equation (2), the artifact-free MI-EEG neural signal is obtained via equation (12).

$$\hat{x} = z - \widehat{W}^T z \tag{12}$$

D. GEVD-MWF Artifact Removal Procedure

Compared with the number of EEG channels, the potential artifact sources (represented as Q) are usually very small, so the rank of the covariance matrix P_{yy} is typically low. However, in reality, the estimated matrix $\hat{P}_{yy}$ is generally equal to N rather than Q and it may even not be positive semi-definite due to the subtraction $\hat{P}_{zz} - \hat{P}_{xx}$ [28]. Consequently, performing the mean subtraction by incorporating a low-rank approximation based on a GEVD forces $\hat{P}_{yy}$ to be positive semi-definite thereby enhancing the estimation performance of the MWF, especially in low SNR conditions [29]. Because both P_{zz} and P_{xx} are symmetric and positive definite, an invertible Matrix U, in which the columns are normalized and the generalized eigenvectors are defined, is obtained in equation (13).

$$\sum_x = U^T P_{xx} U\,, \quad \sum_z = U^T P_{zz} U \tag{13}$$

where $\sum_z$ and $\sum_x$ are the real-valued diagonal matrices with $\sum_z = diag(\alpha_{z1}, \alpha_{z2}, \ldots, \alpha_{zN})$ and $\sum_x = diag(\alpha_{x1}, \alpha_{x2}, \ldots, \alpha_{xN})$ defining the generalized eigenvalues. To perform the GEVD of the ordered matrix pair $(\hat{P}_{zz}, \hat{P}_{xx})$, each generalized eigenvector and its corresponding generalized eigenvalue, U_N and λ_N(n=1,2,…,N) need to be computed in such a way that $P_{zz}U_N = \lambda_N P_{xx}U_N$ [32], which is equivalent to equation (14).

$$P_{zz}U = P_{xx}U \Lambda \tag{14}$$

Equation (14) is referred to as the GEVD and it could be observed that it extracts the directions with maximal SNR. Similarly, computing the GEVD is the same as finding the joint diagonalization of P_{zz} and P_{xx}. Therefore, with the diagonalization in equation (14), we have the following:

$$\begin{aligned} P_{yy} &= U^{-T} \sum_z U^1 - U^{-T} \sum_x U^{-1} \\ P_{yy} &= U^{-T} (\sum_z - \sum_x) U^{-1} \\ P_{yy} &= U^{-T} \sum_y U^{-1} \end{aligned} \tag{15}$$

where $\sum_y = diag(\alpha_{y1}, \alpha_{y2}, \ldots, \alpha_{yN})$ and $\alpha_{yi} = \alpha_{zi} - \alpha_{xi}$.

Since P_{yy} has rank Q, only the first Q diagonal elements of $\hat{\sum}_y$ will be non-zero. However, as $\hat{P}_{yy}$ generally doesn't have rank Q, the GEVD is used to compute a rank-Q approximation for P_{yy}. Thus, the GEVD of ($\hat{P}_{zz}$, $\hat{P}_{xx}$) and $\hat{P}_{yy}$ are calculated where the last N-Q diagonal elements of $\sum_y$ are replaced by zeros [11, 29].

In reality, Q is usually unknown, so there are several known methods to set the rank of $\hat{P}_{yy}$. In this study, we adopt the conventional method of setting the negative entries in $\hat{\sum}_y$ to zero, to avoid using non-positive semi-definite covariance matrix estimation. One of the desirable characteristics of the proposed method is that it is completely unaffected by the scaling and linear combination of the input signals (the output signals and SNR are independent of the scaling and combination), hence making it possible to capture the highest signal to noise ratio in the signals [31].

The proposed method was implemented with the aid of EEGLAB and MATLAB tools in a manner that integrates a graphical user interface, enabling visualization of the MI-EEG signals for efficient processing of their spatio-temporal characteristics [11]. The operational procedure of the proposed method involves marking and extracting artifact segments in the signals using a graphical interface, as shown in Figure 3. Afterward, the statistical properties of the extracted segments are learned and automatically applied to remove artifact components in the subsequent unmarked portion of the signals. To optimally eliminate multiple artifacts while preserving the rich set of neural information in the MI-EEG signals, full marking with a broad margin was applied while marking the artifact segments, thus offering the advantage of automatic cancellation of various inherent artifacts in the signals (Figure 3).

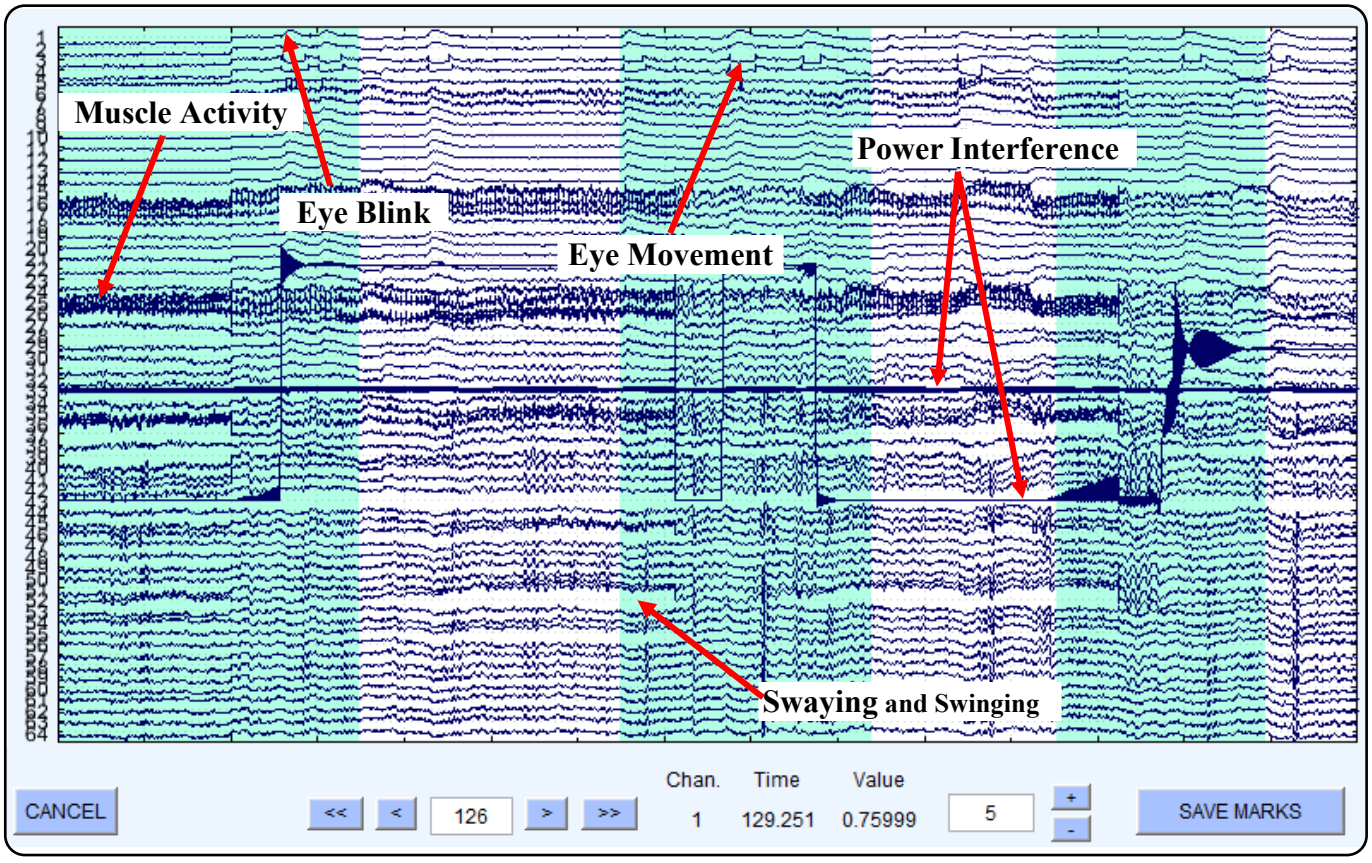

Figure 3: A representation of the multiple artifact marking process (such as eye blink, eye movement, power interference, muscle activity and swaying and swing) using a custom graphical user interface

This addresses the problem of partial marking adopted by most existing artifact removal methods, which often leads to errors in the estimation of $\hat{P}_{xx}$ as presented in equation (8). In this regard, the recorded MI-EEG signals were visually inspected and a subset of example segments that were considered artifacts (as shown in Figure 3) were marked, saved, and exported to MATLAB for further processing. The flow chart diagram in Figure 4 represents the artifact removal procedure by the proposed method.

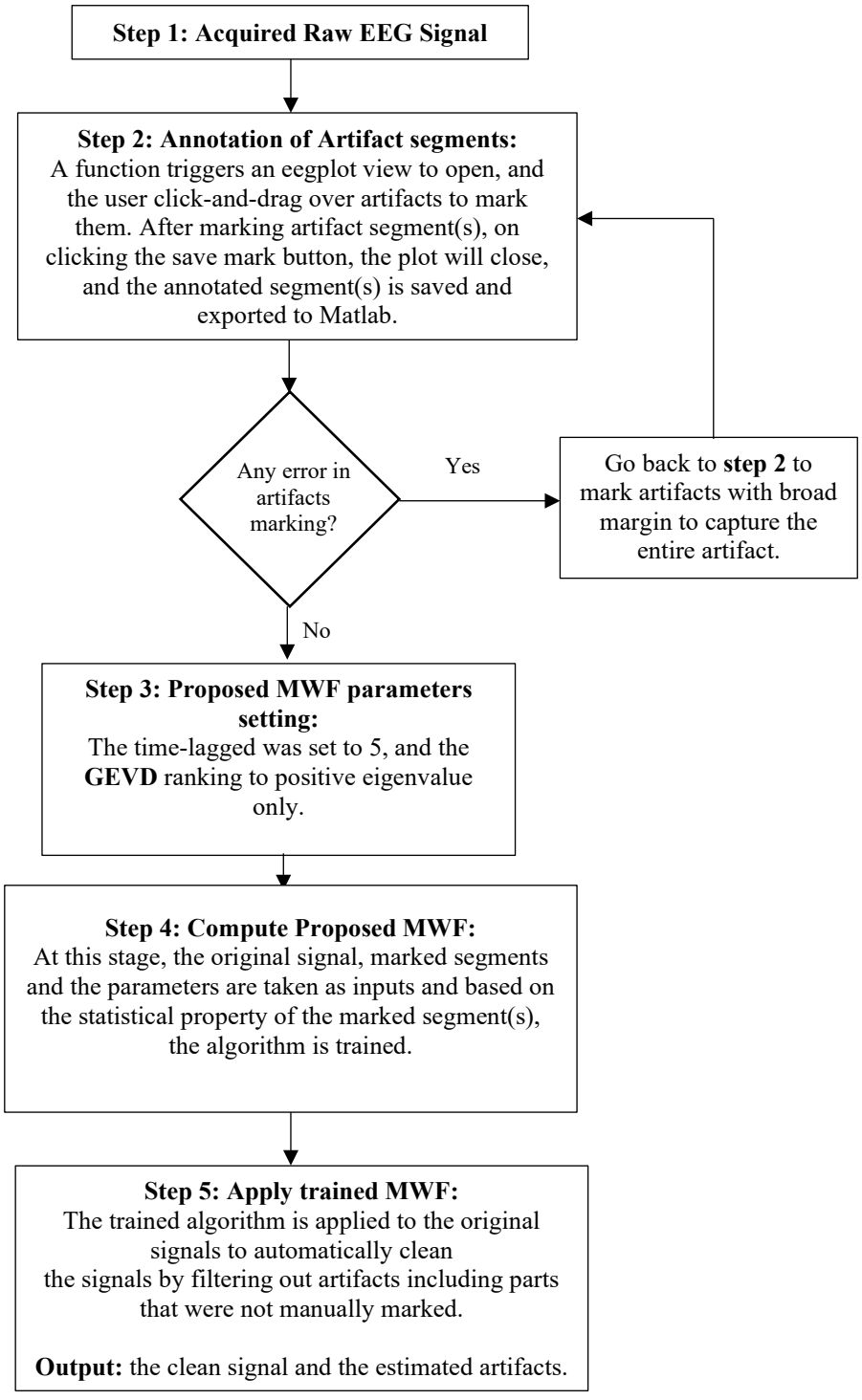

Figure 4: A flowchart of the proposed multi-artifact removal operational procedure

The performance of the proposed method was compared with the following commonly utilized artifact removal methods:

a) MARA (Multiple Artifact Rejection Algorithm): a supervised machine learning algorithm developed to handle eye artifacts, muscular artifacts, and loose electrodes [33].
b) ADJUST (An Automatic EEG artifact Detector based on Spatial and Temporal features): an algorithm developed to capture blinks, eye movements, and generic discontinuities [34].
c) InfoMax: a classical ICA method that uses higher-order statistics to remove stereotypical artifacts such as eye movements, blinks, and cardiac activity [35].
d) Adaptive threshold filtering (ATF): a conventional method that incorporates adaptive thresholding, and notch filters to remove artifacts such as eye movements, blinks, and power interference [3].

It is worth noting that, before the MARA and ADJUST methods were applied to the MI-EEG signals, the signal was first filtered and preprocessed with ICA, as outlined in [33-34].

E. Channel Selection based on vSFFS Algorithm

Generally, multichannel EEG signals contain a large amount of redundant information that does not contribute to signal classification and instead incurs additional noise and increased computational cost and equipment setup time [36]. Channel selection algorithms can be applied to effectively exclude these redundant channels by selecting a set of optimal channels with the higher neural information density required for accurate decoding of MI tasks [37-39]. In this respect, this study implemented a variant of the sequential forward floating Selection (vSFFS) algorithm to eliminate redundant channels without affecting the classification performance of the MI tasks. Specifically, the vSFFS algorithm incorporated a thresholding mechanism that helps determine its stopping criteria more efficiently during execution. Unlike conventional SFFS, the vSFFS employed in this study minimizes the number of iterations in selecting subsets of channels by removing and/or adding channels which helps saves time and computing resources. And its selection criteria is based on maximizing the prediction accuracy and was found to be cost-effective in terms of computational complexity and accuracy.

Suppose C, Y_m, J(Y_m) represent the full set of EEG channels, an empty channel subset of m channels, and the performance, in terms of accuracy, of the subset, Y_m, respectively. The selection process begins with an empty channel subset (m = 0), whereby each channel in C is evaluated. After each iteration, a channel is added to the subset Y_m if it increases the prediction accuracy, otherwise it is removed. This process continues until a predefined stopping criterion is reached. In this study, the iteration stopped when the current maximum accuracy was greater than the previous maximum accuracy and the difference between both accuracies was less than $\alpha = 0.002$. The flow diagram in Figure 5 presents a concise description of the vSFFS operational procedure.

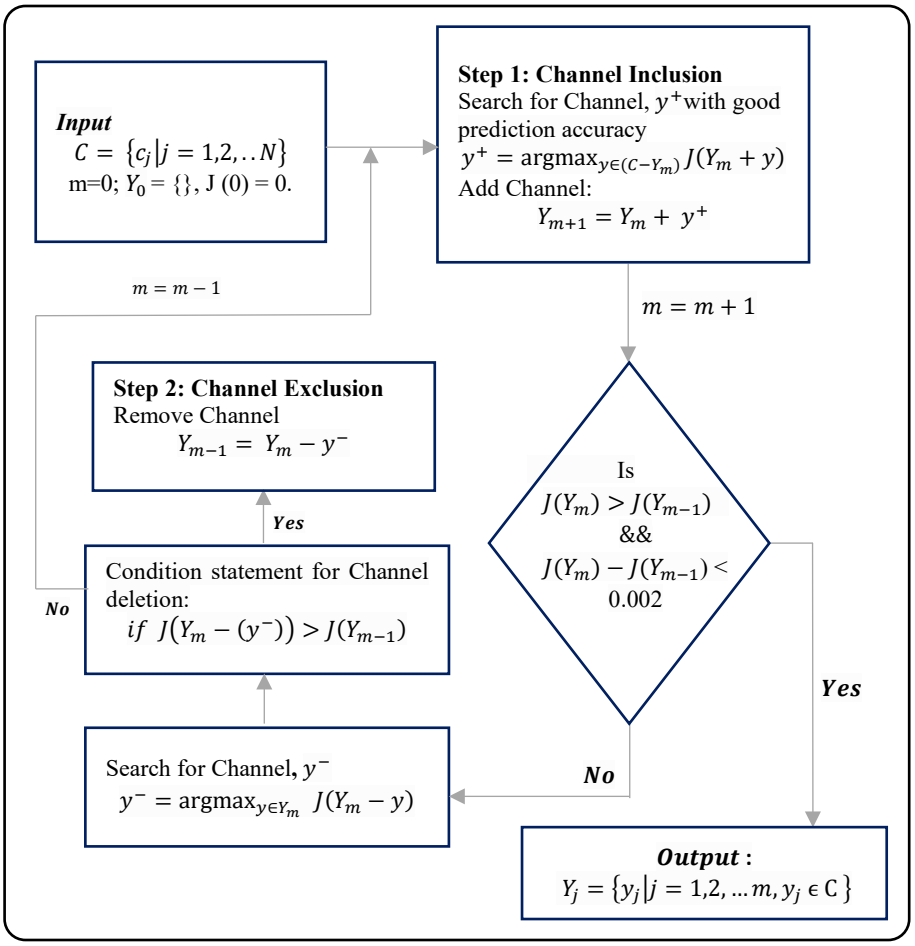

Figure 5: The process flow diagram of the variant sequential floating forward selection algorithm.

F. Feature Extraction and MI Tasks Decoding

After preprocessing the MI-EEG recordings the resulting signals were sliced into smaller segments using overlapping analysis windows of 150ms length with increments of 100ms. Five different feature sets commonly used to characterize movement intents were considered. These included the novel time-domain feature (NTDF) [40], the time-dependent spectral domain features (TD-PSD) [41], Hudgins classical four time-domain descriptors (TD4), [42], the root means square descriptor (RMS), and the 5th order autoregressive coefficients (AR5) [43]. Each set was individually extracted to characterize the five classes of MI tasks contained in the preprocessed EEG signals. Also, these features have been widely considered in the space of EMG signal pattern characterization. However, findings from our previous studies have shown that these features can also be extracted from EEG signals to characterize the inherent information of interest [3, 44]. Therefore, adopted a set of time-domain features due to their relative simplicity in terms of computation and capability to offer good enough decoding accuracy [3, 44], which aligns well with the objective of our study.

To decode the MI tasks, the extracted MI-EEG feature vectors were classified using four conventional machine learning classifiers; linear discriminant analysis (LDA), support vector machine (SVM), artificial neural network (ANN), and k-nearest neighbors (kNN). These classification algorithms were adopted because they have been

shown to yield high classification accuracy with good generalization capabilities in terms of MI-EEG signal decoding [45]. A 5-fold cross-validation framework was used to partition the MI-EEG features vector into training and testing sets to evaluate each of the above classifiers.

G. Performance Evaluation and Statistical Analysis

To evaluate the performance of the proposed and existing methods, the classification accuracy (CA) and geometric mean (GM) were utilized as described below. The CA metric measures the performance of the classifier in terms of its capability to correctly predict all of the classes of MI-EEG tasks. And it is the ratio of the number of correctly classified samples to the total number of test samples, as expressed in equation (16). The GM measures the balance between the classification performance on the majority and minority classes, providing vital information for determining the overfitting of the true positive classes or underfitting of the negative classes. Consequently, the GM is computed as a function of the sensitivity and specificity, as shown in equations (17) and (18).

$$Classification\ accuracy\ (CA) = \frac{Number\ of\ correctly\ classified\ samples}{Total\ number\ of\ testing\ samples} * 100\% \tag{16}$$

$$Sensitivity = \frac{TP}{TP + FN}\ ,\quad specificity = \frac{TN}{TN + FP} \tag{17}$$

$$Geometric\ mean\ (GM)\ =\ \sqrt{sensitivity \times specificity} \tag{18}$$

where TP is the number of true positives correctly predicted as positive, TN is the number of true negatives correctly predicted as negative, FP is the number of true negatives predicted as positive, and FN is the number of true positives predicted as negative, as obtained from a confusion matrix.

Also, normalized correlation function expressed in equation (19) was adopted to evaluate the signal pattern estimation capability of the proposed and existing methods.

$$Corr\_norm_{x,y} = \frac{\sum_{n=0}^{N-1} x[n]\, y[n]}{\sqrt{\sum_{n=o}^{N-1} x^2\,[n]} \sum_{n=o}^{N-1} y^2\,[n]} \tag{19}$$

where x and y represent the data points in original signal and cleaned signal respectively (cleaned signal from the proposed and existing preprocessing methods) while N is the length of the signal

One way analysis of variance (ANOVA) and paired sample t-tests were used to evaluate the statistical significance of the obtained results while Cohen's D was used to measure the effect size between the means of the proposed and the existing methods. Notably, a confidence level of $p<0.05$ was employed, and all statistical analyses were performed using the Sigma plot software (version 14.0).

III. RESULTS

A. Performance Evaluation of the EEG Preprocessing Methods

The average classification performances across subjects and MI tasks when the MI-EEG signals were preprocessed with the proposed method or the other considered methods are shown in Figure 6a-6d. For each preprocessing method, the five feature sets described in **section II.F** were extracted from the signals and the MI tasks were decoded using each of the four classifiers (LDA, SVM, ANN, and KNN).

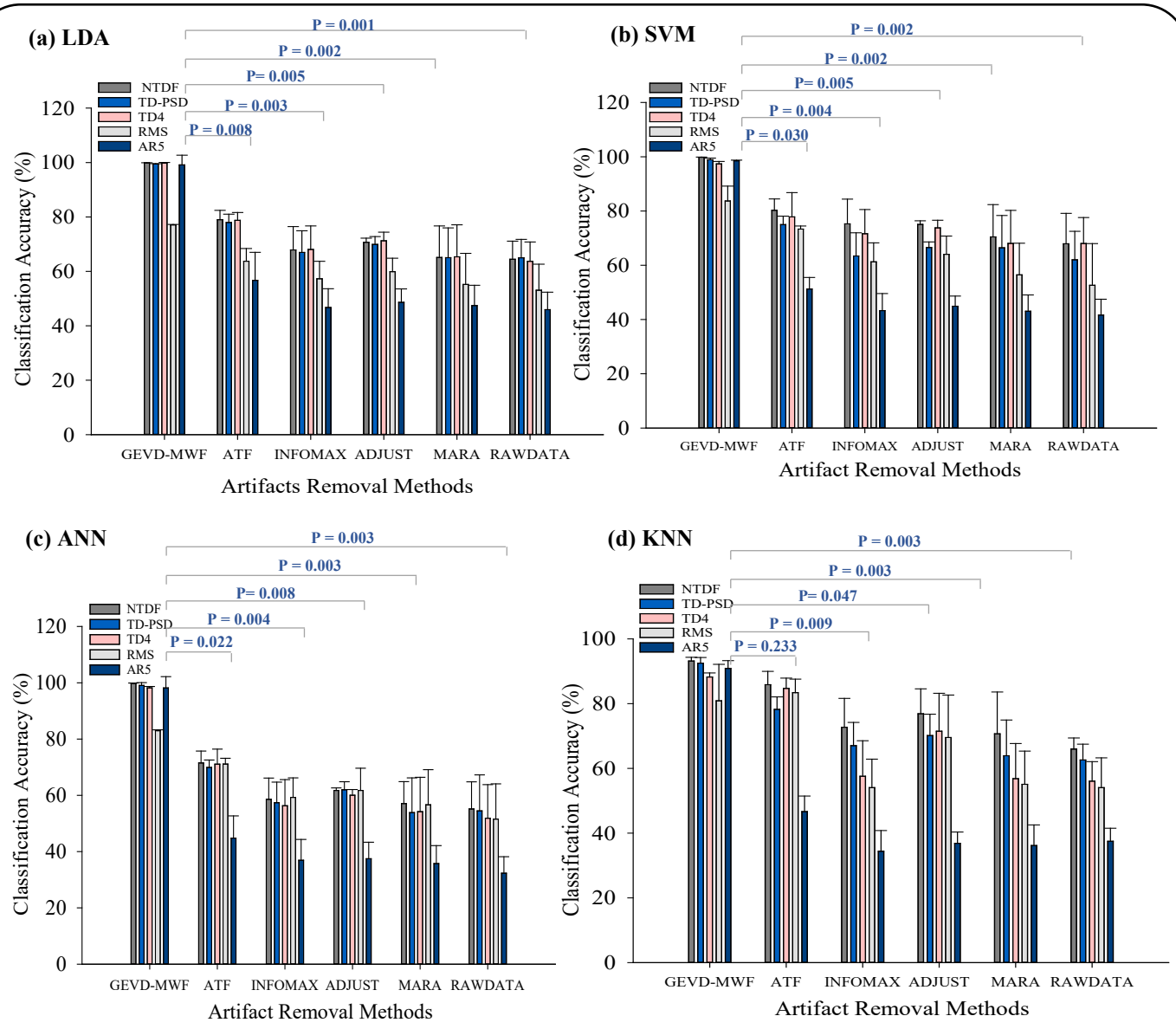

Figure 6: The average classification performance of the proposed method and comparison methods across all subject and classes of MI tasks for LDA (a) SVM (b) ANN (c) and KNN

Compared to existing EEG artifact removal methods, the proposed GEVD-MWF method can be seen to achieve the highest average classification performance in decoding the MI tasks across the different features and classifiers (Figure 6a-6d). Note that the square bracket across each preprocessing method indicates the pairwise t-test

comparison between the proposed and other existing methods with the corresponding p-value displayed above it. From the analyses in Figure 6a-6d, it can be observed that the improved performance of the proposed method over all other methods was statistically significant ($p<0.05$) for all the classifiers, except in Figure 6d (KNN) where there is no significance between GEVD-MWF and the ATF method ($p = 0.233$), despite noticeable improvement. Also, from the Cohen's D effect sizes reported in Table 2, it can be seen that the proposed method has very large improvement effects, across all classifiers, further signifying the effectiveness of the proposed method.

Table 2: A comparison of Cohen's D effect size between the proposed method and considered preprocessing methods, and the raw signals for different classifiers

S/No.		***Cohen'D Effect size values***				***Mean***
1	**Methods Comparison**	**LDA**	**SVM**	**ANN**	**KNN**	
2	GEVD-MWF & ATF	2.33	2.35	2.63	0.98	**2.07±0.74**
3	GEVD-MWF & INFOMAX	3.47	3.74	4.33	2.74	**3.57±0.66**
4	GEVD-MWF & ADJUST	3.12	3.43	3.71	1.89	**3.04±0.80**
5	GEVD-MWF & MARA	3.89	4.24	4.71	3.11	**3.99±0.68**
6	GEVD-MWF/RAWDATA	3.92	3.99	4.82	3.68	**4.11±0.50**
	Mean	**3.35±0.59**	**3.55±0.66**	**4.01±0.8**	**2.48±0.95**	

Note: Cohen suggested that $d = 0.2$ be considered a 'small' effect size, 0.5 represents a 'medium' effect size, and that values above 0.8 denote a 'large' effect size.

Overall, the proposed method led to substantial improvements in classification accuracy in the range of 24.07% - 36.03% for LDA, 23.73% - 37.12% for SVM, 13.23% - 31.32% for ANN and 28.92% - 41.21% for KNN compared with the existing methods (ATF, INFOMAX, MARA, and ADJUST) and the original signal. Unlike the proposed GEVD-MWF approach, which yielded classification accuracies as high as 99.89%, 99.83%, 99.77%, and 93.19% for the NTDF feature across the four classifiers, respectively, it can be deduced from these results that the previous methods were unable to adequately handle artifacts inherent in the MI-EEG signals, leading to substantially lower decoding outcomes for the MI tasks, regardless of classifier or feature sets.

In the second phase of the evaluation, we investigated the performance of the various preprocessing methods and the original signal using the geometric mean metric for each combination of feature set and classifier, as shown in Table 3a-3d. These results reveal a performance trend consistent with the analyses in Figure 6a-6d, where the proposed method recorded the highest geometric mean values across all feature extraction methods and classifiers except for the KNN classifier with ATF preprocessing, which achieved similar results for the TD4 and RMS features with no significant difference ($p>0.05$). These analyses (classification accuracy and geometric mean) demonstrate that the proposed GEVD-MWF method enables the extraction of accurate and stable features for the classification of MI-EEG tasks.

Table 3: Average performance based on Geometric mean metric for the proposed and conventional EEG signal processing methods across subject and classes of MI tasks for LDA (a) SVM (b) ANN (c) and KNN

(a) LDA	GEVD-MWF	ATF	INFOMAX	ADJUST	MARA	RAWDATA
NTDF	1.00 ± 0.00	0.87 ± 0.02	0.79 ± 0.06	0.81 ± 0.01	0.77 ± 0.08	0.72 ± 0.04
TD-PSD	1.00 ± 0.00	0.86 ± 0.02	0.78 ± 0.06	0.80 ± 0.02	0.77 ± 0.08	0.62 ± 0.04
TD4	1.00 ± 0.00	0.86 ± 0.02	0.79 ± 0.06	0.81 ± 0.02	0.77 ± 0.08	0.72 ± 0.04
RMS	0.85 ± 0.00	0.76 ± 0.03	0.71 ± 0.05	0.73 ± 0.04	0.70 ± 0.09	0.66 ± 0.07
AR5	0.99 ± 0.02	0.71 ± 0.08	0.64 ± 0.05	0.65 ± 0.04	0.64 ± 0.06	0.53 ± 0.05
Mean	**0.97± 0.01**	**0.81 ± 0.03**	**0.74 ± 0.06**	**0.76 ± 0.02**	**0.73 ± 0.08**	**0.65 ± 0.05**

(b) SVM	GEVD-MWF	ATF	INFOMAX	ADJUST	MARA	RAWDATA
NTDF	1.00 ± 0.00	0.87 ± 0.03	0.79 ± 0.06	0.81 ± 0.01	0.78 ± 0.08	0.76 ± 0.08
TD-PSD	0.99 ± 0.00	0.84 ± 0.02	0.76 ± 0.06	0.78 ± 0.01	0.75 ± 0.09	0.61 ± 0.07
TD4	0.98 ± 0.01	0.67 ± 0.01	0.81 ± 0.06	0.83 ± 0.02	0.79 ± 0.09	0.75 ± 0.06
RMS	0.90 ± 0.04	0.88 ± 0.03	0.74 ± 0.05	0.76 ± 0.05	0.71 ± 0.09	0.64 ± 0.11
AR5	0.99 ± 0.00	0.83 ± 0.07	0.61 ± 0.05	0.62 ± 0.03	0.61 ± 0.05	0.50 ± 0.04
Mean	**0.99 ± 0.01**	**0.82 ± 0.03**	**0.74 ± 0.06**	**0.76 ± 0.02**	**0.73 ± 0.08**	**0.65± 0.07**

(c) ANN	GEVD-MWF	ATF	INFOMAX	ADJUST	MARA	RAWDATA
NTDF	1.00 ± 0.00	0.81 ± 0.03	0.72 ± 0.05	0.75 ± 0.01	0.71 ± 0.09	0.65 ± 0.07
TD-PSD	0.89 ± 0.12	0.80 ± 0.02	0.72 ± 0.05	0.75 ± 0.02	0.69 ± 0.08	0.65 ± 0.09
TD4	0.99 ± 0.00	0.81 ± 0.04	0.71 ± 0.07	0.74 ± 0.01	0.69 ± 0.08	0.63 ± 0.08
RMS	0.89 ± 0.00	0.81 ± 0.01	0.73 ± 0.05	0.75 ± 0.06	0.71 ± 0.07	0.63 ± 0.09
AR5	0.99 ± 0.03	0.62 ± 0.06	0.56 ± 0.06	0.56 ± 0.05	0.55 ± 0.06	0.50 ± 0.05
Mean	**0.95 ± 0.03**	**0.77 ± 0.03**	**0.69 ± 0.06**	**0.71 ± 0.03**	**0.71 ± 0.08**	**0.61± 0.07**

(d) KNN	GEVD-MWF	ATF	INFOMAX	ADJUST	MARA	RAWDATA
NTDF	0.96 ± 0.01	0.91 ± 0.03	0.82 ± 0.06	0.85 ± 0.05	0.81 ± 0.09	0.73 ± 0.01
TD-PSD	0.95 ± 0.01	0.86 ± 0.03	0.78 ± 0.05	0.81 ± 0.04	0.76 ± 0.08	0.70 ± 0.02
TD4	0.88 ± 0.08	0.90 ± 0.02	0.72 ± 0.08	0.81 ± 0.08	0.71 ± 0.08	0.67 ± 0.02
RMS	0.88 ± 0.08	0.89 ± 0.03	0.69 ± 0.06	0.80 ± 0.09	0.70 ± 0.07	0.67 ± 0.03
AR5	0.94 ± 0.02	0.64 ± 0.04	0.53 ± 0.06	0.56 ± 0.03	0.55 ± 0.06	0.52 ± 0.05
Mean	**0.92 ± 0.04**	**0.84 ± 0.03**	**0.71 ± 0.06**	**0.77 ± 0.06**	**0.67 ± 0.08**	**0.66 ± 0.03**

B. Estimation of EEG Waveform based on GEVD-MWF and Existing Methods

In this section, the capability of the GEVD-MWF in eliminating artifacts from raw EEG recordings as a function of estimating the underlying signal of interest was investigated in comparison to the existing methods. Hence, a normalized correlation analysis technique was applied to the signals obtained via the GEVD-MWF and the other existing methods with respect to the original EEG signals. Compared with the existing preprocessing methods (ATF, INFOMAX, ADJUST, and MARA), the GEVD-MWF method was able to better estimate the signal of interest, thereby achieving a high-level of correlation with the original signal (Table 4). In other words, the proposed method

was able to retain and estimate the component of interest from the raw EEG recordings while removing the contaminated artifacts. The estimation outcomes of the GEVD-MWF method yielded the best average correlation value of 0.6514 ± 0.09 across subjects compared to the considered methods, corroborating the overall best classification performance found across classifiers and features (Table 3). Meanwhile, ATF method appears to have obtained the next best result (0.5085 ± 0.10), yielding a relatively better estimation than the remaining previous methods. Notably, a value ranging from -1 to +1 is used to measure the strength and direction of the linear relationship between two continuous samples or signals, especially in the context of correlation analysis.

Table 4: Signal estimation capability using normalized correlation analysis between the raw signal and each of the preprocessing method subject-wise.

SUBJECTS	*GEVD-MWF*	*ATF*	*INFOMAX*	*ADJUST*	*MARA*
Trans-H1	0.5831	0.4117	-0.1861	0.3207	0.1509
Trans-H2	0.6758	0.5056	0.3443	0.6136	0.5726
Trans-H3	0.5867	0.4651	0.4791	0.5385	-0.2093
Trans-H4	0.7601	0.6514	0.6713	0.4765	0.4152
Mean	**0.6514 ± 0.09**	**0.5085 ± 0.10**	**0.3272 ± 0.43**	**0.4873 ± 0.12**	**0.2324 ± 0.34**

In summary, the proposed GEVD-MWF can be observed to have better artifact cancellation and signal estimation capability both qualitatively and quantitatively compared to the other methods, providing further justification for the performance of the proposed method that was shown in Figure 6 and Table 2. A one-way ANOVA test was performed on the correlation analyses result in Table 4; the test showed statistical significance ($P = <0.001$). All pairwise multiple comparison procedures using Bonferroni t-test were carried out to check which comparison between the methods is significant, and the result showed that there is statistical significance between GEVD-MWF vs. MARA ($p < 0.001$) and GEVD-MWF vs. INFOMAX ($p = 0.004$). Meanwhile, there is no significance between the proposed method and the other two methods (ATF and ADJUST). Based on the consistently superior performance of the proposed method as measured from multiple perspectives, we focus subsequent analyses solely on the evaluation of the proposed method. Therefore, the feasibility of applying the proposed method on a single-trial EEG recording with a fewer number of electrode channels, which are considered to be essential for real-time processing of brain information in practical applications was investigated. Also, due to the low performance of RMS features and inconsistency across classifiers, it was excluded from the subsequent results presented in this study.

C. Performance of the GEVD-MWF across Single and Multiple Trials

The use of EEG signals from a single experimental trial (or at least very few) is essential for MI-EEG BCI systems to be translated to real-life applications. Nevertheless, most existing MI-EEG-based movement intent decoding methods are built based on ensembles of multiple trials, limiting their applicability in terms of real-time processing. Thus, we investigated the possibility of achieving a robust MI decoding with a minimum possible number of trial(s)

using the proposed GEVD-MWF method, as this may offer potential insights about the applicability of the method for real-time MI task decoding. That is, we applied the proposed method to a range of trials from 1 to 5 and then examined the extent to which the MI tasks could be decoded across feature sets and classifiers (Figure 7a-7d).

Analysis of the results obtained from a single trial (1-Trial) shows MI decoding accuracies of 96.21%, 99.67%, 97.98%, and 90.44% when using NTDF features with LDA, SVM, ANN, and KNN classifiers, respectively. It can also be seen that, intuitively, the MI decoding accuracies increased with the number of trials. However, statistical testing indicated that there is no significant effect when using SVM ($p > 0.2973$) or KNN ($p > 0.301$). Conversely, a significant effect was found for LDA ($p < 0.0000084$) and ANN ($p < 0.014$), with post-hoc t-tests showing significant differences for the LDA between the 1-Trial and 5-Trials case, and ANN between the 1-Trial and 4-Trials. It is worth noting that the comparison was carried across the group of trials and not across feature sets. These results provide compelling evidence for the potential of rapid and accurate processing using the GEVD-MWF method in practical applications.

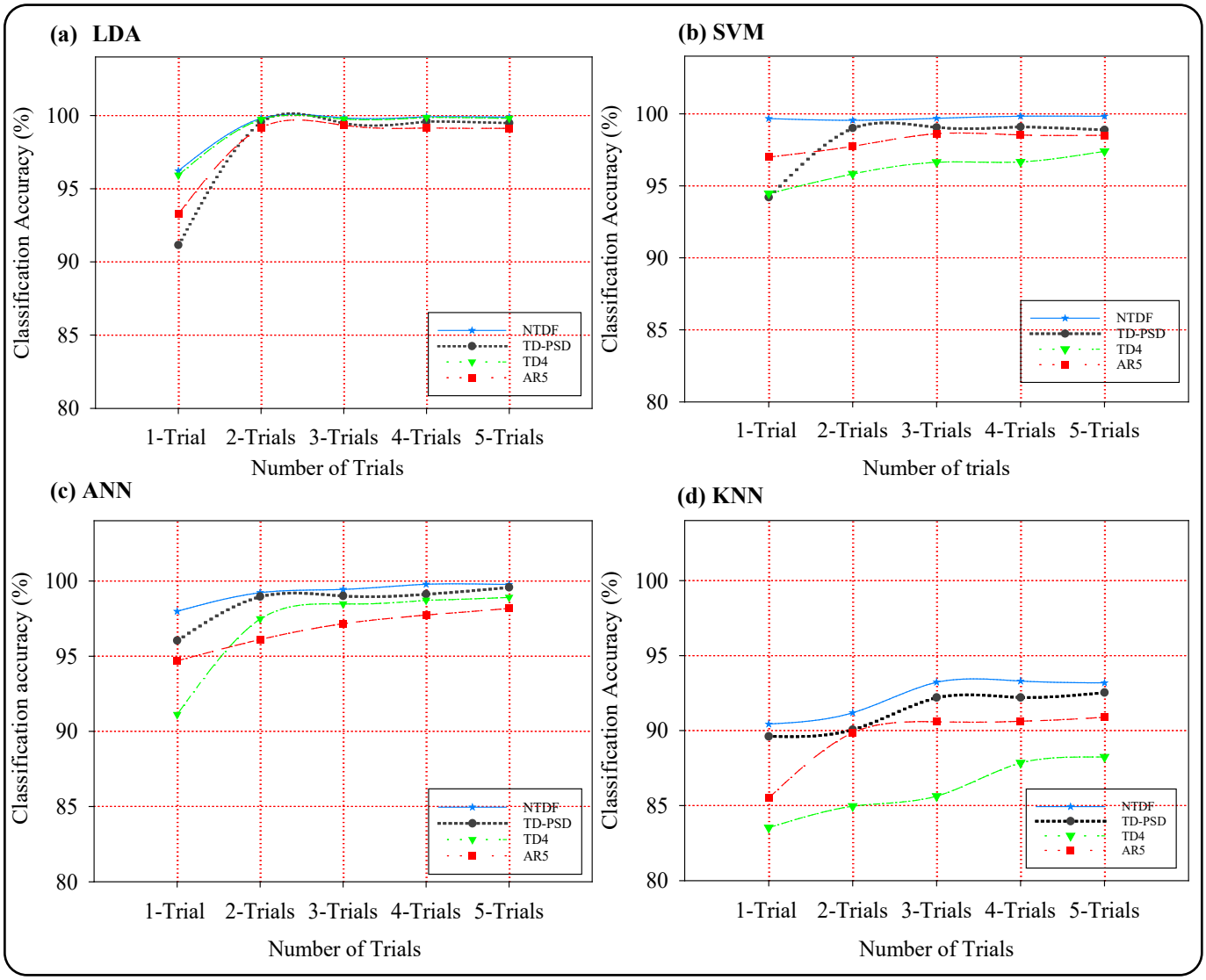

Figure 7: The average classification performance of the proposed method and comparison methods across all subject and classes of MI tasks for a) LDA, b) SVM, c) ANN, and d) KNN

Although the GEVD-MWF method effectively eliminates artifacts from single and multiple trials of EEG recording, it appears to pair particularly well with NTDF features and SVM classifier when classifying MI based on a single trial of EEG.

D. Selection of Optimal Channel Subsets

For efficient and effective use of MI-EEG signals in clinical settings, there is motivation to reduce the necessary set of channels. Consequently, an optimal subset of highly relevant channels that could maximize information density, reduce overfitting and computation, and minimize set-up times in practical applications is of interest. Therefore, the possibility of adopting the proposed GEVD-MWF method when using information from a subset of EEG channels constructed using the previously described vSFFS algorithm was investigated. That is, after applying the GEVD-MWF preprocessing method to the MI-EEG signal recording, the vSFFS algorithm was utilized to construct a reduced subset of electrodes from the 64 original EEG channels. Following the application of GEVD-MWF to each subject's original EEG signals, the vSFFS channel selection was applied using a KNN classifier. Data were first partitioned into training and testing sets (in the ratio of 70:30) to select optimal channels that contribute most to the decoding of inherent MI tasks. The outcome of the channel selection process is shown in Figure 8a-8d, where a subset of 9 best channels was constructed by the vSFFS algorithm from the original 64-EEG channels for each subject.

In general, it can be observed that the first four channels led to significant improvement in MI decoding accuracy, with diminishing returns for subsequent channels. The locations of the selected channels for each of the transhumeral amputee subjects are shown in Figure 8 using topographic maps.

The topographic map represents the color-coded contours of brain activity characteristics, which provide a spatial view of the modulation frequency or/and amplitude of the EEG modulations co-registered to the scalp position. The topographic analysis shown in Figure 8a-8d highlights the regions of the brain responsible for pattern/movement intentions elicited by the four transhumeral amputee subjects. Based on the preprocessed data using our proposed method, weights were assigned to each subject's 64 channel data using EEGLAB tool, thereafter the assigned weight was used to generate the topography map with the aid of a built-in function. It is worth noting that the intensity of the color ranges from blue (less contributive channels) to red (more contributive channels) as shown in the map legends. Detailed analysis of these maps revealed that the locations of the optimally selected electrodes varied across individual subjects, suggesting that an initial investigation to determine the best locations on the scalp may be necessary in clinical or research settings.

To further explore this concept, a cross-validation approach was adopted to evaluate the generalizability on subject-specific basis. Briefly, the 9-channel subset determined using dataset of Trans-H1 was applied to decode the MI tasks of all 4 subjects using their respective data from those locations. Similarly, this procedure was repeated using the 9-channel subsets for each of the other subjects, yielding the classification results shown in Table 5.

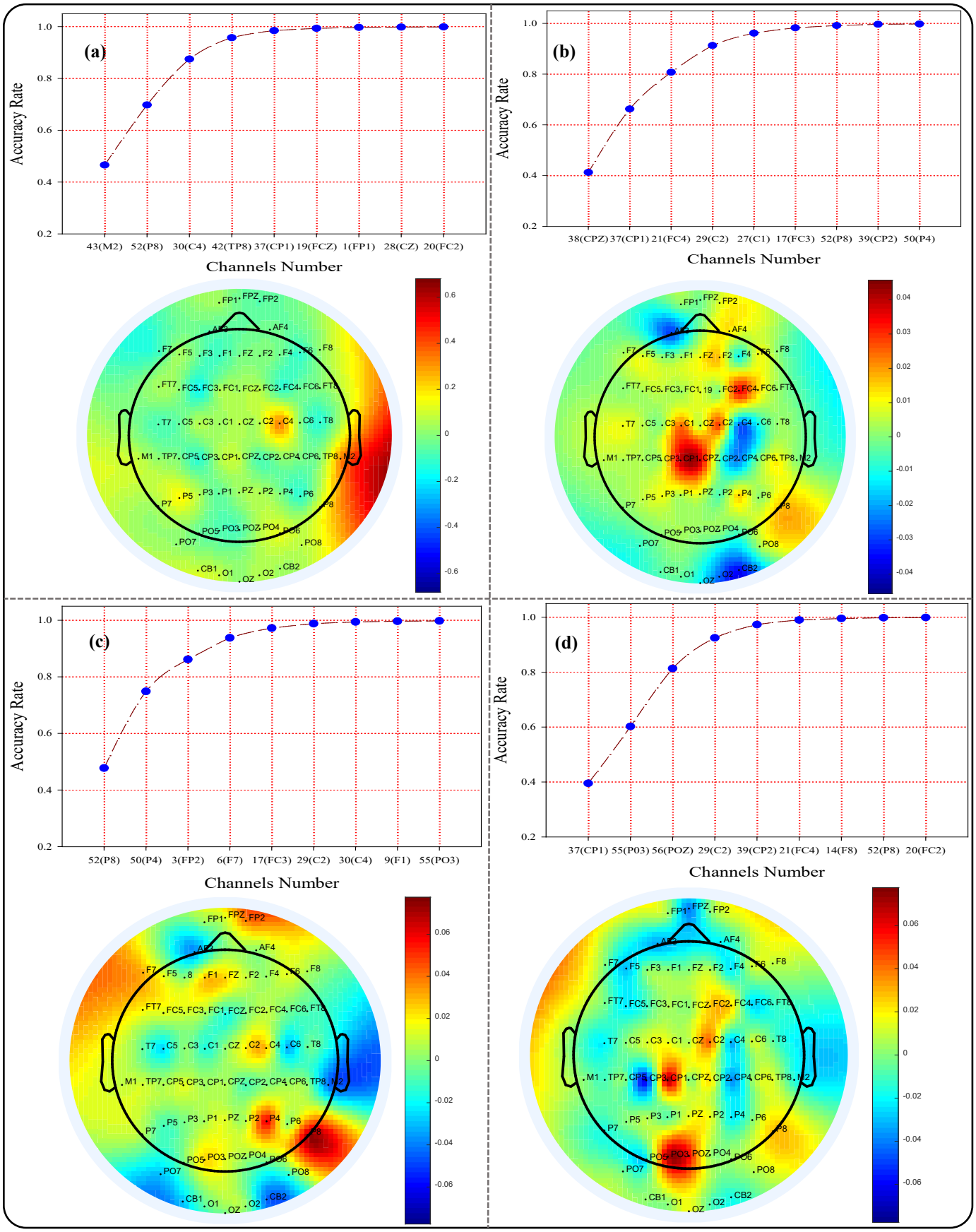

Figure 8: Channel selection graphs and topography plots for participants (a) Trans-H1 (b) Trans-H2 (c) Trans-H3 and (d) Trans-H4, using the vSFFS channel selection algorithm. Each panel shows the location of the optimal electrodes for the subjects and the decoding accuracies for a corresponding MI task.

Due to the consistently high performance of the NTDF feature set in the previous results, it was used here in combination with the proposed preprocessing method before decoding using the LDA, SVM, ANN, and KNN classifiers (Table 5). Note that Table 5 reports the average classification performance across MI tasks. It can be seen that the 9-channel subset determined using dataset of Trans-H2 achieved the highest generalization performance across all participants and was thus adopted for subsequent evaluation in this study.

Table 5: Average classification results (%) across MI tasks, when using the 9-channel subset determined for each of the four subjects.

S/No.	Optimal Subset Channels	LDA	SVM	ANN	KNN
1	Trans-H1	94.84±0.52	93.62± 0.87	91.90± 1.29	83.70±3.16
2	**Trans-H2**	**99.08±0.60**	**97.37± 1.49**	**95.90± 1.79**	**87.97±3.74**
3	Trans-H3	93.19±0.80	94.67±0.48	92.46±0.71	81.93±2.26
4	Trans-H4	95.95±1.84	92.64±1.26	91.03±1.19	82.44±3.81

Note: The 9-channel subset (CPZ, CP1, FC4, C2, C1, FC3, P8, and CP2 AND P4) using the dataset of Trans-H2 generalized far better than the others.

E. Reduced Channels with a Single Trial

Combining the previous two sections to compose a potentially clinically viable configuration, the performance of the proposed method was evaluated when using a single trial recorded from the 9-channel subset determined above (CPZ, CP1, FC4, C2, C1, FC3, P8, CP2 and P4). The obtained results are shown in Figure 9a-9b. Figure 9a depicts the mean classification accuracy of the combinations of feature sets and classifiers for all MI tasks and subjects. Comparing the classification accuracy of the feature sets, across all the classifiers, it can be seen that the combination of NTDF feature and SVM classifier is again better than the other features and classifiers, although with no significant difference ($p<0.05$). As shown by the confusion matrix in Figure 9b, the combination of GEVD-MWF with NTDF and SVM achieved high classification accuracy across tasks (93.69%, overall).

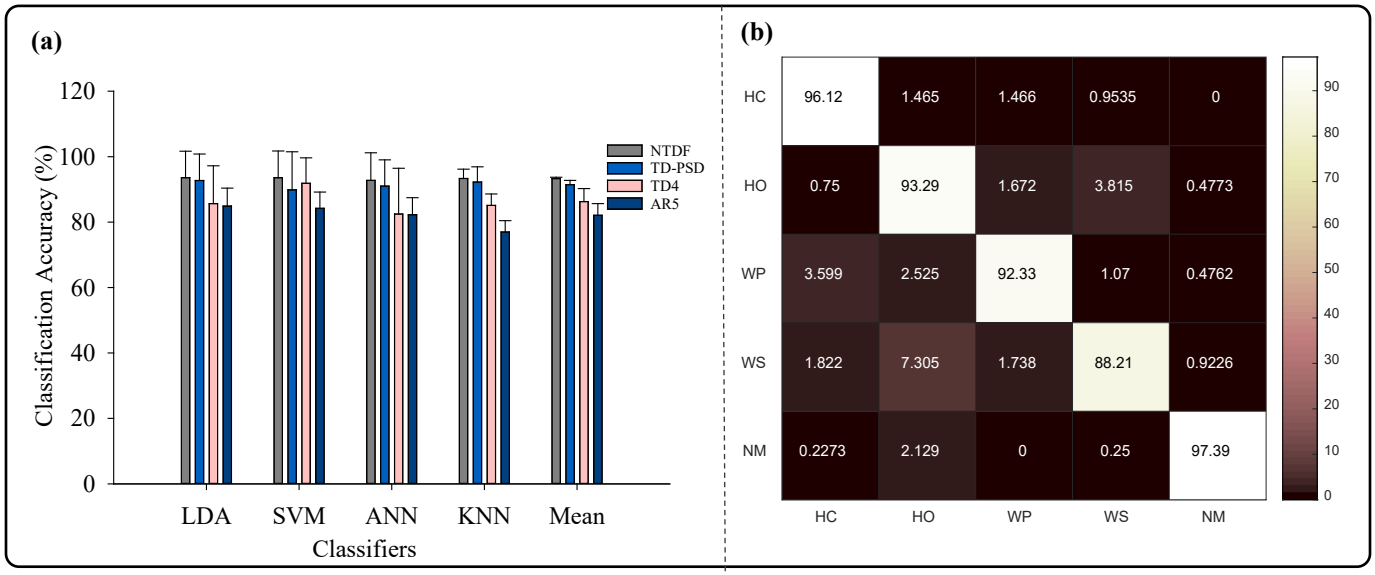

Figure 9: Mean classification performance when using the reduced 9-channel subset with a single trial (a) across all MI tasks and subjects, and (b) of individual MI tasks across all subjects using SVM classifier and NTDF feature.

IV. Discussion

The decoding of MI tasks from multichannel EEG recordings particularly for persons with above-elbow amputations has been limited due to the presence of multiple artifacts (with known and unknown sources) that contaminate the MI-EEG signals. Efforts have been made to develop artifact removal algorithms that could be adopted for use in practical applications, but with only marginal success reported to date [46, 47]. To resolve this issue, a novel MI-EEG preprocessing method (GEVD-MWF), that integrates generalized eigenvalue decomposition driven by low-rank approximation and multi-channel Wiener filter is proposed for improved elimination of multiple artifacts from EEG signals recordings. The performance of the proposed GEVD-MWF method and other notable existing EEG signal preprocessing methods were investigated and compared in terms of their capability to eliminate inherent artifacts using different salient feature sets and classifiers with the obtained results presented in Figure 6a-6d. Analysis of the results shows that the proposed GEVD-MWF achieved significantly better performance ($p < 0.05$) when compared to other existing methods.

For instance, across subjects, MI tasks, features sets, and classifiers, the GEVD-MWF method recorded an overall average MI decoding accuracy of 93.73±1.58% compared with other methods. Meanwhile, the NTDF feature set obtained the highest average MI decoding accuracy when combined with the proposed method across classifiers. Further analysis using the geometric mean metric (Table 3) revealed a similar performance trend, which corroborated these findings, as shown in Figure 6. Observations from both results show that the GEVD-MWF approach for EEG signal preprocessing exhibits stable and robust characteristics in terms of multiple artifact elimination. One possible reason for the consistently accurate performance of the GEVD-MWF method is the use of the interpretable graphical user interface which allows proper annotation and marking of artifacts in EEG recordings from which the statistical properties are automatically learned and applied to remove similar artifacts from the subsequent unmarked portions. By comparison, existing methods based on ICA require identification of artifact components in the transformed space. This can be done automatically or semi-automatically, e.g. using additional topographic plotting to facilitate the assessment of the spatial distribution of the components, thus limiting their usage in practical applications. It is also worth noting that the holistic approach employed by the proposed GEVD-MWF enables it to eliminate artifacts from both neural and non-neural sources, as compared to current methods that are designed to remove single or multiple artifacts from known neural [11].

Although the importance of developing MI-EEG systems based on "*single-trial*" recordings (rather than "*ensembles of trials*") to facilitate real-time processing of neural information in practical applications is widely known, few studies have focused on this approach with limited MI decoding performance reported to date [48-49]. This inspired us to compare the proposed method's performance using both "*single-trial*" EEG recordings and "*ensembles of trials*" to validate its potential applicability in practical settings. The performance shown in Figure 7a-7d suggests that the proposed GEVD-MWF method performs well even on "single-trial" data across a range of subjects and classifiers, yielding MI decoding accuracies in the range of 90.44%-99.67%; substantially higher than those previously reported using single trials. Statistical analysis revealed that there were no significant differences in performance when using reduced trials for two of the four classifiers SVM ($p = 0.2974$) and KNN ($p = 0.3001$).

The KNN classifier recorded the worst performance while SVM achieved the best performance. Although, the LDA classifier showed significant differences based on the number of trials used ($p<0.001$), but it appears to be the most stable classifier across groups of trials and feature sets. In general, these results suggest that the proposed GEVD-MWF method can effectively eliminate multiple artifacts irrespective of the number of trials of EEG recordings used. More importantly, it can be seen that a "single-trial" EEG recording can be used to achieve satisfactory results, effectively eliminating the need to collect ensembles of EEG trials-this could have potentially substantial implications for practical use with prosthetic devices and other BCI systems.

Considering the cost of using large numbers of EEG channels (e.g. computation and setup times and the financial cost of sensors) [3], a vSFFS algorithm was successfully used to select optimal subsets of channels from the original 64-channel EEG recordings with negligible changes in MI decoding accuracy. The graph showing the optimal channel subsets for each subject, shown in Figure 8a-8d, reveals that even after only 5 channels are selected, remarkable accuracies are obtained in the range of 0.9615% - 0.9848%. There were no obvious increments gained for the subsequent channels suggesting that signals from the later channels add less neural information for MI task decoding. Consequently, although results are reported here for 9-channel subsets, even smaller numbers of electrodes may be sufficient. The topographic maps further show that the regions of the brain where the selected channels were located varied across subjects, albeit with some overlapping channels. One reason for this observed difference can be due to the natural reorganization of the brain that occurs after amputation, which can override parts previously dedicated to movement (the motor cortex region) for other activities [38]. It is possible that, with early intervention with MI-EEG based interfaces after amputation, this reorganization could be reduced. Nevertheless, it was observed that most of the generalizable set of channels determined from Subject 2 were located over the motor cortex region.

Finally, the feasibility of adopting the proposed GEVD-MWF method for MI task decoding using a subset of channels *and* a "single-trial" EEG recording was investigated. This combination could facilitate real-time processing in BCI systems to develop a usable prosthetic control interface for above-elbow amputees. In this regard, we studied GEVD-MWF performance using single-trial experiments with the most generalizable subset of 9 channels: CPZ, CP1, FC4, C2, C1, FC3, P8, CP2, and P4. Results showed that a remarkable average MI decoding accuracy of 93.69% was achieved when combined with the NTDF features and an SVM classifier (Figure 9a). Additionally, the results of the confusion matrix presented in Figure 9b showed that the HC, HO, WS, and NM classes all obtained decoding results above 92%, with only WS achieving a somewhat lower 88.21% accuracy. Consequently, we have been able to demonstrate that consistently high accurate MI task decoding could be achieved using only 9 channels of EEG from a single trial recording. It is worth reinforcing that the MI-EEG signals were recorded using a commercially available EEG acquisition system but the obtained results are based on an offline analysis.

It is also important to acknowledge that the proposed method is a semi-automatic and semi-supervised method whose process, although clearly beneficial, still requires the manual annotation of a set of exemplar artifacts during the initialization phase. In our ongoing work, we aim to extend the proposed method by making it fully automated

in a manner that it will integrate an artifact detection algorithm able to self-identify artifact-dominated segments in the signal, like the ADJUST, an automatic ICA based approaches for artifact correction [9, 34]. We will then test the performance of the approaches in an online environment. It is noteworthy that some artifact sources (for example noises from neuromodulation) cannot be easily modeled as purely additive. Thus, we hope to investigate the mechanism underlying their occurrence, which would provide us with more insight on how to enhance our current method. Although EEG-based BCI systems are yet to be commercially applicable across a wide range of human-computer interface applications, the commercial, technological, and algorithmic boundaries are steadily being reduced. We anticipate that the proposed method, and possibly others motivated by the approach, may enable the development of low-cost, portable EEG-BCI systems for real-time MI task decoding.

V. Conclusion

This study proposed a robust and extendible EEG artifact removal algorithm that integrates low-rank approximation based on generalized eigenvalue decomposition (GEVD) and a multi-channel wiener filter (MWF) to remove all forms of artifacts contained in EEG recordings acquired from four transhumeral amputee subjects. To validate the effectiveness of our proposed method, comparative experiments with existing methods were conducted and evaluated using different feature sets, performance metrics, and classifiers, with results demonstrating that the proposed method achieved significantly better performance. Investigation of the number of trials needed revealed that the proposed method can effectively eliminate artifacts from even a single trial of EEG for accurate MI task decoding, regardless of the choice of feature extraction methods and machine learning algorithms. Towards the practical implementation of the proposed method with reduced dimensionality and computational complexity, a variant channel selection method based on sequential forward floating selection (vSFFS) was also used to select the most informative channels. Results using a subset of 9 selected channels from a single subject, mostly from the motor cortex region, yielded comparable average classification accuracies that generalized across subjects. Finally, combined results using the proposed method yielded single-trial, 9 channel average classification accuracies above 90%, with strong decoding performance across individual MI tasks. Findings from this study could help inform the design of effective and robust control methods based on EEG pattern recognition for multifunctional prostheses for patients with above-elbow amputations.

ACKNOWLEDGMENT

The research work was supported in part by the National Natural Science Foundation of China under Grants (#U1613222, #82050410452, #81850410557 and #U1913601), Shenzhen Science and Technology Program (#SGLH20180625142402055). Shenzhen Institute of Artificial Intelligence and Robotics for Society. Lastly, Mojisola G. Asogbon Samuel sincerely appreciates the support of a Chinese Government Scholarship (CSC) in the pursuit of a PhD degree at the University of Chinese Academy of Sciences, Beijing, China.

REFERENCES

[1] Bi, L., & Guan, C. A review on EMG-based motor intention prediction of continuous human upper limb motion for human-robot collaboration. Biomedical Signal Processing and Control, 51, 113-127, 2019.

[2] Scheme, E., & Englehart, K. "Electromyogram pattern recognition for control of powered upper-limb prostheses: state of the art and challenges for clinical use," Journal of Rehabilitation Research & Development, 48(6), 643–59, 2011.

[3] Li, X., Samuel, O.W., Zhang, X., Wang, H., Fang, P., & Li, G. "A motion-classification strategy based on sEMG-EEG signal combination for upper-limb amputees," Journal of Neuroengineering and Rehabilitation, 14(1), 2, 2017.

[4] Rashid, M., Sulaiman, N., PP Abdul Majeed, A., Musa, R. M., Ab Nasir, A. F., Bari, B. S., & Khatun, S. "Current status, challenges, and possible solutions of EEG-based brain-computer interface: a comprehensive review," Frontiers in Neurorobotics, June 3, 2020.

[5] Abiri, R., Borhani, S., Sellers, E. W., Jiang, Y., & Zhao, X. "A comprehensive review of EEG-based brain–computer interface paradigms," Journal of Neural Engineering,16:011001. doi: 10.1088/1741-2552/aaf12e, 2019.

[6] Gu, X., Cao, Z., Jolfaei, A., Xu, P., Wu, D., Jung, T. P., & Lin, C. T. "EEG-based brain-computer interfaces (BCIs): a survey of recent studies on signal sensing technologies and computational intelligence approaches and their applications," arXiv preprint arXiv:2001.11337, 2020.

[7] Jiang, X., Bian, G. B., & Tian, Z. "Removal of artifacts from EEG signals: a review. Sensors," 19(5), 987, 2019.

[8] Padfield, N., Zabalza, J., Zhao, H., Masero, V., & Ren, J., "EEG-based brain-computer interfaces using motor-imagery: techniques and challenges". Sensors, 19(6), 1423, 2019.

[9] Urigüen, J. A., & Garcia-Zapirain, B. "EEG artifact removal—state-of-the-art and guidelines," Journal of Neural Engineering, 12(3), 031001,2015.

[10] Anderer, P., Roberts, S., Schlögl, A., Gruber, G., Klösch, G., Herrmann, W., Rappelsberger, P., Filz, O., Barbanoj, M.J., Dorffner, G., et al. "Artifact processing in computerized analysis of sleep EEG—A review," Neuropsychobiology, 40, 150–157, 1999.

[11] Somers, B., Francart, T., & Bertrand, A., "A generic EEG artifact removal algorithm based on the multi-channel Wiener filter," Journal of Neural Engineering, 15(3), 036007, 2019.

[12] Hillyard, S.A., & Galambos, R. "Eye movement artifact in the CNV. Electroencephalography and Clinical Neurophysiol.ogy, 28 (2), 173–182, 1970.

[13] Whitton, J.L., Lue, F., Moldofsky, H. "A spectral method for removing eye movement artifacts from the EEG," Electroencephalography and Clinical Neurophysiology, 44(6), 735-41, 1978.

[14] Wallstrom, G.L.,Kass, R.E., Miller, A., Cohn, J. & Fox, N. Correction of ocular artifacts in the EEG using Bayesian adaptive regression splines. In Case Studies in Bayesian Statistics; Gatsonis, C., Kass, R.E., Carriquiry, A., Gelman, A., Higdon, D., Pauler, D.K., Verdinelli, I., Eds.; Springer: New York, NY, USA, 2002; Vol. 6, pp. 351–356, ISBN 978-0-387-95472-1.

[15] Berg, P., & Scherg, M. "A multiple source approach to the correction of eye artifacts," Electroencephalography and Clinical Neurophysiology, 90(3), 229-241, 1994.

[16] Lins, O. G., Picton, T. W., Berg, P., & Scherg, M. "Ocular artifacts in EEG and event-related potentials I: Scalp topography," Brain Topography, 6(1), 51-63, 1993.

[17] Wallstrom, G. L., Kass, R. E., Miller, A., Cohn, J. F., & Fox, N. A. "Automatic correction of ocular artifacts in the EEG: a comparison of regression-based and component-based methods," International Journal of Psychophysiology, 53(2), 105-119, 2004.

[18] Berg, P. & Scherg, M. "Dipole modeling of eye activity and its application to the removal of eye artefacts from the EEG ad MEG. Clinical Physics and Physiological. Measurement, 12, 49–54, 1991.

[19] Casarotto, S., Bianchi, A.M., Cerutti, S. & Chiarenza, G.A. "Principal component analysis for reduction of ocular artefacts in event-related potentials of normal and dyslexic children," Clinical Neurophysiology, 115, 609–619, 2004.

[20] Delorme, A., & Makeig, S. " EEGLAB: an open source toolbox for analysis of single-trial EEG dynamics including independent component analysis," Journal of Neuroscience Methods, 134(1), 9-21, 2004.

[21] Clercq, W.D., Vergult, A., Vanrumste, B., Paesschen, W.V. & Huffel, S.V. "Canonical correlation analysis applied to remove muscle artifacts from the electroencephalogram," IEEE Transactions on Biomedical Engineering,53, 2583–2587, 2006.

[22] Chan, H. L., Tsai, Y. T., Meng, L. F., & Wu, T. " The removal of ocular artifacts from EEG signals using adaptive filters based on ocular source components," Annals of biomedical engineering, 38(11), 3489-3499., 2010.

[23] Borowicz, A. " Correction of eye-blink artifacts in EEG recordings using wiener filtering," In 2017 Signal Processing: Algorithms, Architectures, Arrangements, and Applications (SPA) , pp. 172-177, 2017. IEEE.

[24] Wang, D., Miao, D., & Blohm, G., "Multi-class motor imagery EEG decoding for brain-computer interfaces." Frontiers in neuroscience, 6, 151, 2012.

[25] Chen, X., Liu, A., Chen, Q., Liu, Y., Zou, L., & McKeown, M. "Simultaneous ocular and muscle artifact removal from EEG data by exploiting diverse statistics," Computers in Biology and Medicine, vol. 88, pp. 1–10, 2017.

[26] Merinov, P., Belyaev, M., & Krivov, E., "The comparison of automatic artifact removal methods with robust classification strategies in terms of EEG classification accuracy." In 2015 International Conference on Biomedical Engineering and Computational Technologies (SIBIRCON), 221-224, 2015.

[27] Kilicarslan, A., Grossman, R. G., and Vidal, J. L. C. "A robust adaptive denoising framework for real-time artifact removal in scalp EEG measurements," Journal of Neural Engineering, 13,026013, 2016. doi: 10.1088/1741-2560/13/2/026013.

[28] Hassani, A., Bertrand, A., & Moonen, M. "GEVD-based low-rank approximation for distributed adaptive node-specific signal estimation in wireless sensor networks," IEEE Transactions on Signal Processing, 64(10), 2557–2572, 2016.

[29] Serizel, R., Moonen, M., Dijk, B.V., & Wouters, J. "Low-rank approximation based multichannel wiener filter algorithms for noise reduction with application in cochlear implants," IEEE/ACM Transactions on Audio, Speech, and Language Processing, 22(4), 785–799, 2014.

[30] SFFS Channel Selection Method. https://github.com/brendanoconnor913/SFFS. Retrieved June 12, 2020.

[31] Ille, N., Berg, P., & Scherg, M. "Artifact correction of the ongoing EEG using spatial filters based on artifact and brain signal topographies," Journal of Clinical Neurophysiology 19(2): 113-124,2002.

[32] Hassani, A., Bertrand, A., & Moonen, M. "Cooperative integrated noise reduction and node-specific direction-of-arrival estimation in a fully connected wireless acoustic sensor network," Signal Processing, 107,68 – 81, 2015.

[33] Winkler, I., Haufe, S., & Tangermann, M. "Automatic classification of artifactual ICA-components for artifact removal in EEG signals," Behavioral and Brain Functions, 7,30-30, 2011.

[34] Mognon, A., Jovicich, J., Bruzzone, L. & Buiatti, M. "ADJUST: An automatic EEG artifact detector based on the joint use of spatial and temporal features," Psychophysiology 48 (2), 229-240, 2011.

[35] Lee, T., Girolami, M., & Sejnowski, T. "Independent Component Analysis Using an Extended Infomax Algorithm for Mixed Subgaussian and Supergaussian Sources" Neural Computation, 11(2), 417–441, 1999.

[36] Feng, J. K., Jin, J., Daly, I., Zhou, J., Niu, Y., Wang, X., & Cichocki, A., "An optimized channel selection method based on multifrequency CSP-rank for motor imagery-based BCI system." Computational Intelligence and Neuroscience, 2019.

[37] Pudil, P., Novovicová, J., & Kittler, J. "Floating search methods in feature-selection," Pattern Recognition Letters, 15(11), 1119–1125, 1994.

[38] Reunanen J., Overfitting in making comparisons between variable selection methods. J Mach Learn Res, 3, 1371–1382, 2003.

[39] Lopes, F. M., Martins-Jr, D. C., Barrera, J., & Cesar-Jr, R. M. "An iterative feature selection method for GRNs inference by exploring topological properties," 2011. arXiv preprint arXiv:1107.5000.

[40] Samuel, O. W., Asogbon, M. G., Geng, Y., Chen, S., Feng, P., Chuang, L., & Li, G. "A novel time-domain descriptor for improved prediction of upper limb movement intent in EMG-PR system," In 2018 40th Annual International Conference of the IEEE Engineering in Medicine and Biology Society , 3513-3516, 2018. IEEE.

[41] Al-Timemy, A.H., Khushaba, R., Bugmann, G., & Escudero, J. "Improving the performance against force variation of EMG controlled multifunctional upper-limb prostheses for transradial amputees," IEEE Transaction on Neural Systems and Rehabilitation Engineering, 24 (6), 650–661, 2016.

[42] Englehart, K., & Hudgins, B. "A robust real-time control scheme for multifunction myoelectric control, IEEE Transactions on Biomedical Engineering, 50 (7) , 848–854, 2003.

[43] Phinyomark, A., Khushaba, R., Ibáñez-Marcelo, E., Patania, A., Scheme, E., & Petri, G. "Navigating features: a topologically informed chart of electromyographic features space, Journal of the Royal Society Interface, 14 (137) , 2017.

[44] Samuel, O. W., Geng, Y., Li, X., & Li, G. "Towards efficient decoding of multiple classes of motor imagery limb movements based on EEG spectral and time domain descriptors," Journal of Medical Systems, 41(12), 1-13, 2017.

[45] Samuel, O.W., Zhou, H., Li, X., Wang, H., Zhang, H., Sangaiah, A.K., & Li, G., "Pattern recognition of

electromyography signals based on novel time domain features for amputees' limb motion classification," Computers and Electrical Engineering, 67, 646-655, 2017.

[46] Sheela, P., & Puthankattil, S. D. "A hybrid method for artifact removal of visual evoked EEG," Journal of Neuroscience Methods, 336, 108638, 2020.

[47] Lemm, S., Blankertz, B., Curio, G., & Muller, K. "Spatio-spectral filters for improving the classification of single trial EEG," IEEE Transactions on Biomedical Engineering, 52, 1541–1548, 2005.

[48] Tang, Z., Li, C., & Sun, S. "Single-trial EEG classification of motor imagery using deep convolutional neural networks," Optik, 130, 11-18, 2017.

[49] Li, L., Xu, G., Xie, J., & Li, M., "Classification of single-trial motor imagery EEG by complexity regularization," Neural Computing and Applications, 1-7, 2019.

2021

A linearly extendible multi-artifact removal approach for improved upper extremity EEG-based motor imagery decoding

Asogbon, Mojisola Grace

IOP Publishing Ltd

https://iopscience.iop.org/article/10.1088/1741-2552/ac0a55